



Optimal design and characterization of sulfide-modified nanoscale zerovalent iron for diclofenac removal



Shikun. Song^{a,b,1}, Yiming. Su^{b,c,d,1}, Adeyemi S. Adeleye^{d,e}, Yalei. Zhang^{a,b}, Xuefei. Zhou^{a,b,*}

^a College of Environmental Science and Engineering, Tongji University, Shanghai 200092, China

^b State Key Laboratory of Pollution Control and Resources Reuse, Tongji University, Shanghai 200092, China

^c College of Civil engineering, Tongji University, Shanghai 200092, China

^d University of California Center for Environmental Implications of Nanotechnology, Santa Barbara, CA, USA

^e Bren School of Environmental Science & Management, University of California, Santa Barbara, 3420 Bren Hall, CA 93106, USA

ARTICLE INFO

Article history:

Received 16 May 2016

Received in revised form 28 July 2016

Accepted 31 July 2016

Available online 1 August 2016

Keywords:

Sulfide-modified nZVI

Diclofenac

Groundwater remediation

Oxygen activation

Sulfidation-driven catalysis

ABSTRACT

Noble metal catalyzed nanoscale zerovalent iron (nZVI) has shown some promise in degrading pharmaceuticals, but it still suffers from inactivation caused by common anions. In this study, sulfidation was adopted to enhance diclofenac (DCF, an emerging groundwater pollutant) removal under aerobic conditions in the presence of common anions. X-ray adsorption near edge structure (XANES) analysis shows that dithionite is not only able to sulfurize nZVI, but also stimulates the crystal growth of Fe(0) and restrains FeOOH formation to some degree. Except in CaCl₂ solution, certain extent of sulfidation can inhibit the aggregation and sedimentation of nZVI in aqueous media with common ions and anions. While pristine nZVI achieves only 21.2% DCF removal, the optimal sulfide-modified nZVI (S-nZVI) shows 73.5% DCF removal under near neutral condition (pH ~6.5), and the maximum removal could reach 85.9% at pH 4.5. Mechanism study shows that a heterogeneous layer composed of iron sulfide and iron oxide restricts the direct reaction between oxygen and Fe(0), but facilitates electron transfer from Fe(0) core to Fe(III), producing considerable amount of surface bound Fe(II). Electron Paramagnetic Resonance spectrometer (EPR) analysis and quenching experiments further demonstrate that sulfidation catalyzes dissolved molecular oxygen activation through one-electron transfer. Moreover, sulfidation can lower the negative impact of common anions and humic acid on DCF removal, and S-nZVI is capable of removing DCF in simulated groundwater efficiently. This study provides fundamental understanding on the sulfur catalyzed oxidation of DCF under aerobic conditions.

© 2016 Published by Elsevier B.V.

1. Introduction

Diclofenac (DCF) is a synthetic non-steroidal anti-inflammatory drug, which is widely used as a pain killer. Due to its widespread use and poor treatability in conventional sewage treatment plants (STPs) [1], DCF has been found in a wide range of environmental circumstances including drinking water, surface water, and groundwater [2–4]. The European Union recently included DCF in the “watch list” of emerging aquatic pollutants, and required its

environmental monitoring in member states [5]. Therefore, efficient technologies for DCF removal are needed.

Nanoscale zeorvalent iron (nZVI), a green in-situ nanomaterials for both organic [6–8] and inorganic [9–11] contaminants removal, has been shown to degrade organic contaminants such as chloramphenicol [12], ibuprofen [13], 4-chlorophenol [14], under aeration conditions effectively. Mechanistic studies show that nZVI can react with molecular oxygen (O₂) to produce reactive oxygen species (ROS) [15–19], but the low yield of ROS production in nZVI/O₂ system restricts its further application. To catalyze ROS generation, organic (such as oxalate, nitrilotriacetic acid, and ethylenediaminetetraacetic acid) [20,21] and inorganic ligands (such as polyoxometalate and polyphosphate) [22–24] have been used. However, these are not stable in the presence of ROS. Modifying electron transfer on the core-shell surface of nZVI is another strategy to enhance ROS generation. Ai et al. [25] synthesized core-

* Corresponding author at: College of Environmental Science and Engineering, Tongji University, Shanghai 200092, China.

E-mail address: zhouxuefei@tongji.edu.cn (Xuefei. Zhou).

¹ These authors contributed equally to this work and should be considered co-first authors.

shell Fe@Fe₂O₃ nanowires, which provided more surface bound ferrous ions to catalyze O₂. Lee et al. [26] a nickel modified nZVI, and found that it yielded more oxidants compared to nZVI by restricting the direct reaction between hydrogen peroxide and the nickel-iron surface, and by catalyzing the reaction between hydrogen peroxide and dissolved Fe(II). Nie et al. [27] introduced cobalt to iron to create a bimetallic catalyst; this enhanced interfacial electron transfer due to the presence of two redox couples (Fe³⁺/Fe²⁺ and Co²⁺/Co³⁺).

Although doped noble metals can boost free radical production, catalyst poisoning is often observed when sulfide or humic acid is present in the reaction system [28]. Sulfidation of nZVI may be a better alternative to noble metal doping due to its electron conductivity [29]. In recent studies, a one-pot sulfidation method to synthesize sulfide-modified nZVI (S-nZVI) was developed and the derived nanoparticles were successfully used for metal removal [30] and rapid dechlorination of trichloroethylene (TCE) [31]. However, the atomic and molecular structure of the nanoparticles, especially the iron-sulfur cluster structure was not elucidated. For O₂ reduction catalysis, not only is the particle composition importance, but also the particle surface and size [32]. Additionally, for the application of nanomaterials in groundwater remediation, the stability of the particles need to be understood as their aggregation and sedimentation behavior may affect their pollutant removal efficiency [33,34]. However, despite a steady growth in the publications demonstrating successful lab-scale application of S-nZVI [29–31,35], systematic studies on surface chemistry, aggregation, and sedimentation behavior of the nanoparticles have not been done.

In this study, we synthesized and characterized S-nZVI nanoparticles with different iron-sulfide ratios, and investigated their reactivity towards DCF under aeration condition. Experiments were conducted over a range of pH conditions (3.5–8.5), in the presence of different anions, and in a simulated groundwater to determine potential applicable conditions for in-situ remediation. This study improves our understanding of the mechanism of O₂ activation by S-nZVI.

2. Materials and methods

2.1. Chemical reagents

Sodium borohydride (NaBH₄, 98%), dithionite (Na₂S₂O₄, 85%), anhydrous ferric chloride (FeCl₃, 99.9%), sodium hydroxide (NaOH, 99.99%), sodium chloride (NaCl, 99%), sodium nitrate (NaNO₃, 99%), sodium sulfate (Na₂SO₄, 99%), sodium bicarbonate (NaHCO₃, 99.7%), nickel sulfate heptahydrate (NiSO₄·7H₂O, 99%), disodium hydrogen phosphate (Na₂HPO₄, 99%), humic acid (HA, technical), hydrochloric acid (HCl, 37%), 5,5-Dimethyl-1-pyrrolidine N-oxide (DMPO, 97%), methanol (HPLC grade, 99.9%), acetic acid (HPLC grade, 99.99%) were purchased from Sigma-Aldrich. Diclofenac sodium (98% purity), was purchased from J&K Chemical Co. Ltd. (Beijing, China). All chemicals were used without further purification. Ultrapure water (18.2 MΩ·cm, Barnstead) was used to prepare all reagents and particle suspensions.

2.2. nZVI, Ni-coated nZVI and S-nZVI synthesis

nZVI, S-nZVI and Ni-coated nZVI were synthesized using methods described previously [26,30]. Briefly, 200 ml containing 7.6 g sodium borohydride and different amounts of dithionite (0, 0.25, 0.5, 0.75, 1.0 g for samples hereafter referred as nZVI, 0.25 S-nZVI, 0.5 S-nZVI, 0.75 S-nZVI and 1.0 S-nZVI, whose S/Fe molar ratio were approximate 0, 0.1, 0.2, 0.3 and 0.4, respectively) were added in a dropwise manner to 200 ml FeCl₃ (4.9 g) solution. For Ni-coated nZVI, nZVI suspension was firstly prepared, followed by addition of

nickel sulfate solution, setting Ni/Fe molar ratio to 0.5. The particles obtained were washed three times using deoxygenated water, and then separated from the aqueous phase using a magnet. Notably, at dosage of 1.0 g dithionite, part of the final material became flocculent, and we collected the magnetic part for this study. Fresh nZVI and S-nZVI nanoparticles were stored in deoxygenated water at 4 °C and used within three days.

2.3. Stability experiments

Stability of particles in natural waters and different salt solutions was investigated via time-resolved aggregation and sedimentation kinetics studies [36,37]. 400 mg/L nanoparticle stock suspensions were bath-sonicated (Branson 2510) for 30 min to disperse the particles. Measured aliquots of nanoparticle stock suspensions, salt (NaCl, NaNO₃, Na₂SO₄, Na₂CO₃, or CaCl₂), and buffer were pipetted into a cuvette, and diluted with DI water (Barnstead NANO pure Diamond, 18.2 MΩ·cm). Final concentration of nanoparticle, salt and buffer for each condition was 50 mg/L, 5 mM, and 5 mM, respectively. For studies in simulated groundwater, no further addition of buffer was performed, and the concentration of nanoparticles was 50 mg/L. Mixing was done via 5 s probe sonication with a Misonix Sonicator S-4000 (QSonica LLC). Aggregation was studied via dynamic light scattering (DLS) using Zetasizer Nano-ZS90 (Malvern, UK). Data were collected in triplicates at 30 s intervals for 1 h. Attachment efficiencies (α) were calculated by normalizing the measured initial aggregation rate constant (k) of particles in a given condition by the diffusion-limited aggregation rate constant, k_{fav} [37]. k_{fav} was determined with nZVI or S-nZVI in the presence of 5 mM CaCl₂. Sedimentation was studied via time-resolved optical absorbency (Shimadzu 1601 UV-vis spectrophotometer).

2.4. Aerobic DCF degradation experiments

The aerobic DCF degradation experiments were carried out at room temperature (25 °C) in 250 ml three-necked flask with bubbling air (800 ml/L). Typically, 6 ml of S-nZVI stock suspension (concentration ~100 g/L) were add to 194 ml solution with 10 mg/L DCF to initiate reaction. ORP and pH were monitored in real time. In experiments to determine the role of pH, solution pH was kept constant by 0.1 mM HCl or NaOH. Aliquots were collected at time intervals using syringes, and immediately filtered with 0.22 μm nylon syringe filters for high performance liquid chromatography (HPLC, Agilent 1200, Japan) analysis. In order to determine the effectiveness of aeration alone in DCF degradation, control experiments were set up in a similar manner but with no addition of S-nZVI. All the degradation experiments were conducted in triplicates.

2.5. Quenching experiments

In these experiments, various amount of quenching reagents were selectively used to quench different types of ROS. *tert*-butanol was used to scavenge all the hydroxyl radical (•OH) produced in the reaction system [38], and iodide ion was used to scavenge surface-bounded •OH. Sulfate radical (•SO₄[−]) formation was probed using ethanol, which is a well-known quenching agent for both •OH and (•SO₄[−]) [39]. Superoxide radical (•O₂[−]) was scavenged by 1,4-benzoquinone (BQ).

2.6. DCF removal tests in simulated groundwater

In this part, the initial concentration of DCF was set to 2 mg/L, anion concentration was set to 1 mM, and 5 mg/L humic acid was added to simulate naturally-occurring groundwater situation [40]. For better comparison, the simulated groundwater recipe is

the same as the study on TCE removal by S-nZVI [31], which is composed of NH₄Cl (1 mM), MgCl₂ (0.05 mM), MnCl₂ (0.02 mM), NaCl (0.12 mM), CaCl₂ (6 mM), Na₂HPO₄·2H₂O (0.45 mM), KH₂PO₄ (0.15 mM), Na₂SO₄ (1 mM), and NaHCO₃ (1 mM) [41]. Initial pH of groundwater was set at 6.5.

2.7. Analytical methods

The concentration of DCF was determined by HPLC using following conditions: Phenomenex Gemini C₁₈ 250 × 4.6 mm (particle size 5 μm) column; mobile phase consisted of 82% CH₃OH and 18% water (containing 1% acetic acid) at a constant flow rate of 1.0 ml/min, with UV detection wavelength set at 276 nm. The concentration of Fe(II) and total iron was measured by 1,10-phenanthroline method using a UV-vis spectrometer (Shimadzu, UV-2550, Japan) at 510 nm [42], and hydrogen peroxide (H₂O₂) concentration was determined by iodometric titration method [43]. A fraction of all the samples was freeze-dried for X-ray diffraction (XRD, Bruker D8 Advance) and X-ray photoelectron spectrometry (XPS, Kratos Ultra) analyses. Transmission electron microscopy (TEM, FEI Titan 300 kV FEG) was employed to investigate the structure of the nanoparticles. Electron paramagnetic resonance (EPR) spectra were obtained using a Bruker EMX 10/12 spectrometer with DMPO as a spin-trapping agent. Reactions were scaled down to 10 ml for tests, and methanol was used as reaction solution for •O₂⁻ detection test, because of its disproportionation in water. Fe K-edge X-ray absorption near edge structure (XANES) measurements were carried out on beamline BL 14W at Shanghai Synchrotron Radiation Facility (Shanghai, China). A Si(1 1 1) crystal monochromator was utilized to monochromatize the white beam. The storage ring energy was run at 3.5 GeV with injection currents of 200 mA. Before analyzing samples, the monochromator was calibrated through Fe foil measurement.

3. Results and discussion

3.1. Nanoparticle composition with different extents of sulfidation

XANES results for the synthesized S-nZVI particles with different dithionite treatments are shown in Fig. 1. The linear combination fits (LCF) data show that the proportion of Fe(0) in the final nanoparticles slightly increases from 83.5% to 90.8% as the amount of dithionite added during synthesis increases from 0 to 0.5 g, and then decreases progressively at higher dosage. It is very likely that the stronger bond between Fe and S over Fe and O [44] effectively suppresses the formation of Fe-O upon sulfidation. That is to say, the reaction between Fe(0) and H₂O (or DO) during synthesis is restrained [45], and more Fe(0) can be preserved. Increasing dithionite dosage during synthesis leads to the increase of FeS content in final materials from 7.5% to 13.7% (except at the highest dithionite concentration, which may result from the fact that part of material became nonmagnetic and only the magnetic part was collected for experiments and analysis), which may subsequently lead to the decrease of Fe(0). It's interesting to observe the content change of unordered Fe-O bond under different conditions. In accordance with our previous study, the Fe(0) nucleation during synthesis of nZVI and highly sulfurized nZVI was different: the former was directly from Fe²⁺ ions reduction; the latter was from Fe-O (in precipitation) reduction [46]. Hence, Fe-O bond content variation indicates a transition of the Fe(0) nucleation pattern. As seen in the XANES data, the disappearance of the FeOOH shell and the high content of Fe(0) may contribute to the improvement of TCE and pertechnetate (TcO₄⁻) removal performance [31,47].

Table 1
Attachment efficiencies (α) of nanoparticles in different solutions.

	S-nZVI	nZVI
No salt	0.030	0.033
NaCl	0.051	0.048
NaNO ₃	0.013	0.057
Na ₂ SO ₄	0.057	0.061
Na ₂ CO ₃	0.034	0.139
Groundwater	0.170	0.147

3.2. Micro-structure of S-nZVI

A TEM image of freshly prepared 0.75 S-nZVI is shown in Fig. 2. Compared with nZVI (~60 nm, Fig. S1), the core-shell structure of S-nZVI is somewhat deteriorated, which is corroborated by the disappearance of FeOOH in XANES analysis. In line with our previous study [30], S-nZVI has large spherical particles (~270 nm) covered by considerable amount of FeS_x flakes. The large size of S-nZVI particles is ascribed to the suppression of Fe(0) nucleation, and the bloom of Fe(0) crystal growth resulting from Na₂S₂O₄ addition [48].

Interestingly, the typical nano-chain structure of nZVI [33] formed through van der Waals forces, electrical double layer interactions, and the magnetic attractive force [33,49], is not observed in S-nZVI. In this study, we compared the zeta potential and saturation magnetization (Ms) of nZVI and S-nZVI, and found that S-nZVI had high surface charge (Fig. S2) but low Ms (Fig. S3), which meant electrostatic repulsion was enhanced but magnetic attraction weakened. Additionally, as can be seen in Fig. 2, the increased distance between particles resulting from the presence of FeS_x flakes may also impart some steric stability on S-nZVI nanoparticles.

3.3. Aggregation and sedimentation behavior of S-nZVI

The aggregation behavior of nZVI/S-nZVI in solution with common ions found in groundwater is illustrated in Fig. 3a–c. Notably, the aggregation of S-nZVI was not as rapid as that of nZVI in Na salts, although 5 mM CaCl₂ caused rapid aggregation of both nanoparticles due to absolute suppression of electrostatic repulsion between the particles [49]. The attachment efficiencies (α) of both nanoparticles derived from these conditions are provided in Table 1. Low levels of Cl⁻, and SO₄²⁻ have a weak influence on the aggregation of both nanomaterials due to limited compression of the electrical double layer, which is in agreement with previous studies [50]. However, there is a clear difference in aggregation behavior induced by CO₃²⁻ between nZVI and S-nZVI. Sulfidation makes surface bound Fe(II) exist as FeS, which means CO₃²⁻ cannot bind with Fe(II) since the solubility coefficient of FeS is much lower than FeCO₃ [44]. Whereas, with nZVI, CO₃²⁻ compress the electrical double layer, and induces fast aggregation. We surprisingly find that NO₃⁻ improves the stability of S-nZVI in aqueous media as shown by a lower α in the presence of NaNO₃ than in pure water. According to zeta potential analysis, S-nZVI is more stable at higher pH (>8) (Fig. S2). Coincidentally, NO₃⁻ can be reduced by Fe(0) (Eq. (1)), and this reaction can bring the pH from ~8 to over 9 (data not shown) [51]. Hence, NO₃⁻ may enhance electric repulsion among nanoparticles, which subsequently lowers aggregation of S-nZVI.



Rapid aggregation of nanoparticles results in faster sedimentation due to a greater gravitational force with larger particles ([36,37]; Fig. 3d). Generally, nZVI settles down more quickly than S-nZVI, except for 5 mM CaCl₂ (after 25 min). Ca²⁺ ions are not only able to enter into the double electrode layer, but also able to bind with SO₄²⁻/SO₃²⁻ on S-nZVI surface [44], both of which bring down the surface potential and therefore accelerate the S-nZVI sedimenta-

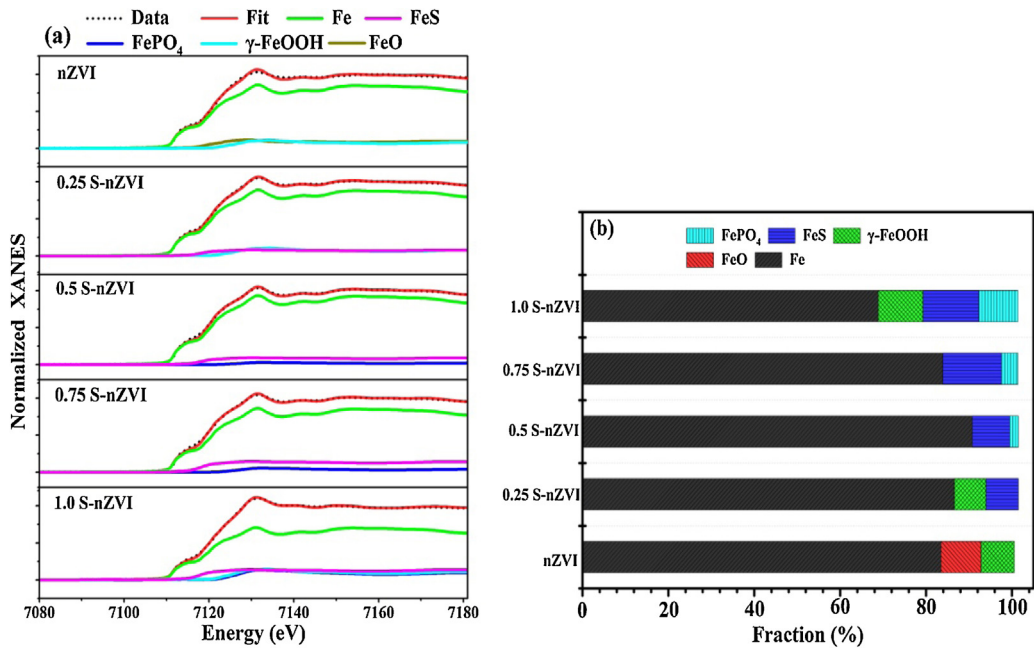


Fig. 1. Fe K-edge XANES linear combination fit (LCF) for different types of S-nZVI (a); fraction of iron species in different S-nZVI (b). (FePO₄ represents unordered Fe—O bond).

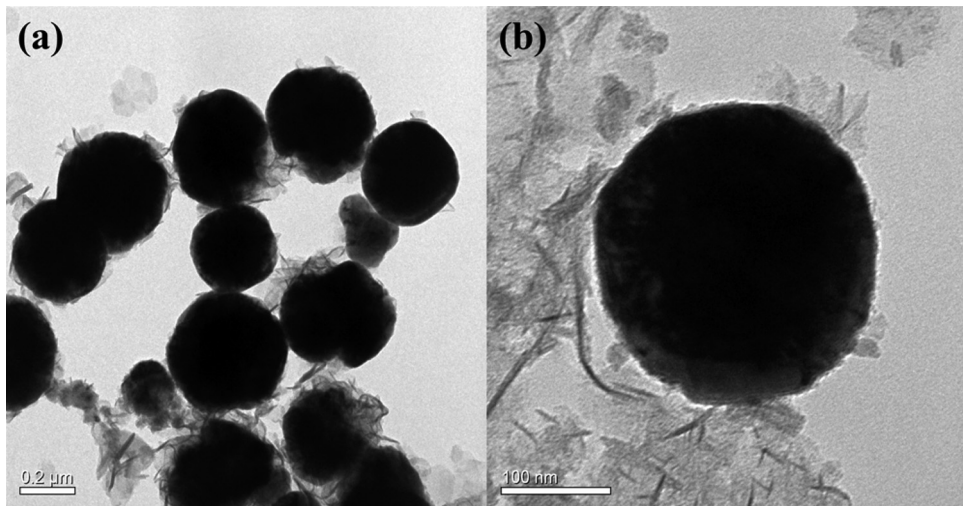


Fig. 2. TEM images of freshly prepared 0.75 S-nZVI.

tation. These aggregation and sedimentation results indicate that sulfidation suppresses the aggregation and sedimentation of nZVI to some extent, which can facilitate the transport of nanoparticles in subsurface [52].

3.4. DCF removal with different S-nZVI

DCF removal results are shown in Fig. 4. No DCF removal is observed with aeration only (data not shown); nZVI or S-nZVI must be present. In consistence with our previous study [30], XPS analysis shows that sulfidation of nZVI is achieved by the addition of dithionite, and iron sulfide compounds (FeS/FeS₂) were identified on surface (Fig. S4). The removal of DCF under aerobic conditions increases from 21.2% to 73.5% as the S/Fe molar ratio increases from 0 to 0.3; and then decreases to 51.4% when it reaches 0.4. The lag time prior to DCF removal is mainly due to the high pH caused by nanoparticles addition initially (Fig. S5), which restrains ROS production (confirmed by EPR studies below). Therefore, S-nZVI from

the synthesis system with molar ratio of S/Fe = 0.3 (0.75 g dithionite addition) is regarded as the optimal S-nZVI for DCF removal (except otherwise noted, S-nZVI refers to 0.75 S-nZVI in the rest of this manuscript).

The different DCF removal ratios among the S-nZVI particles may be due to different contents of Fe(0) in the core and/or FeS in the shells. While Fe(0) content of nZVI is close to that of S-nZVI, DCF removals for these two different nanomaterials are different. The results imply that rather than Fe(0) content, FeS in the shell is the critical factor for efficient DCF removal. In accordance with the literature, FeS can influence the reactivity of S-nZVI with contaminants in at least two ways. First, FeS is a well-known metallic conductor due to the presence of delocalized electrons in its layers [29]. Kim et al. [29] found that the deposition of FeS on nZVI surface can facilitate electron conduction from the Fe(0) core to the surface. Second, FeS is less hydrated than FeO [29], and thus DCF adsorption on the S-nZVI surface is easier than on nZVI. However, above a certain threshold (molar ratio of S/Fe = 0.3), dithionite addi-

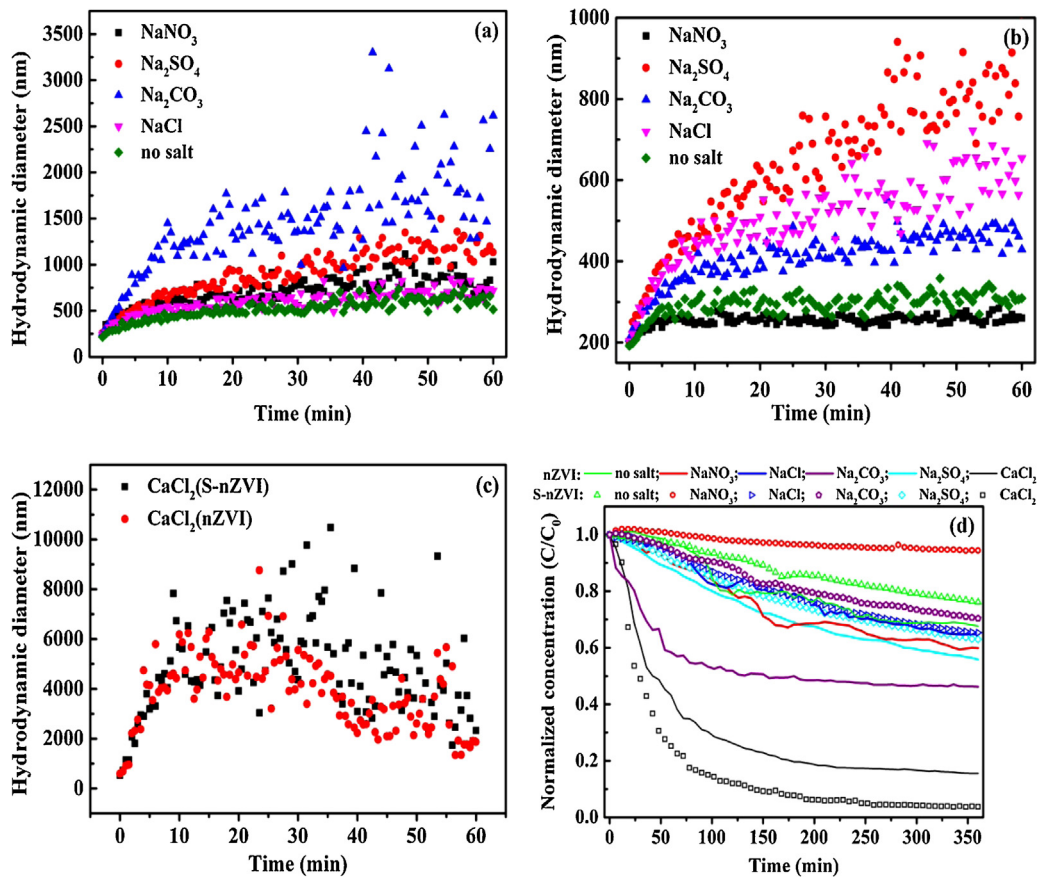


Fig. 3. Aggregation trend of nZVI (a) and S-nZVI (b) in pure water or solution with NaCl, NaNO₃, Na₂CO₃, Na₂SO₄, or CaCl₂ (c); sedimentation trend of nZVI and S-nZVI in different solutions (d).

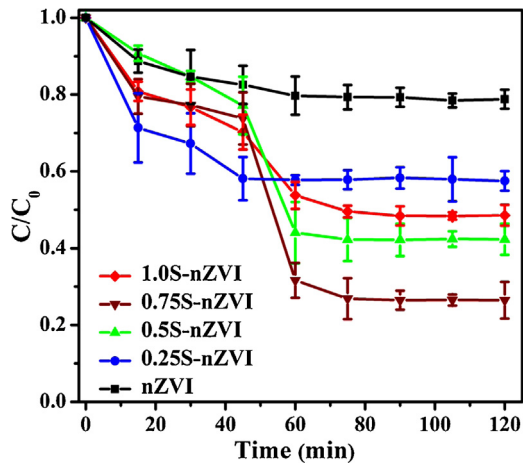


Fig. 4. Removal of DCF by S-nZVI with different extents of sulfidation under aerobic conditions (the dosage of S-nZVI was 3.0 g/L, and the concentration of DCF was 10 mg/L).

tion leads to a decrease of FeS but the increase of FeO indicated by the XANES analysis, both of which are unfavorable to DCF adsorption. Additionally, Fe(0) content decrease may also impair the DCF removal performance since Fe(0) is an effective electron donor for redox reactions.

To further investigate the role/function of iron sulfide on electron transfer, XRD and TEM were used to exam both nZVI and S-nZVI particles composition after reaction (Fig. S6 and Fig. S7); detailed information can be found in Supplementary information. A higher

ratio of γ -FeOOH was obtained in the final products of S-nZVI system, which is typically the final product of Fe species oxidation in water [53] (Eqs. (2) and (3)). The results demonstrate that FeS on S-nZVI surfaces contributes to electron conduction from the Fe(0) core to the surface bound Fe(III), making the best use of inner Fe(0). The results again corroborate our earlier assumption that sulfidation facilitates electron transfer, and thus accelerates oxidation of Fe(0).



To compare the capacity of the mixed shell (made from iron sulfide and iron oxide) in catalyzing O₂ reduction with that of normal iron oxide shell (typically found in pristine nZVI), we conducted EPR analysis for detecting (1) $\bullet\text{O}_2^-$ (DMPO-OOH: $a^{\text{H}} = 12.1\text{ G}$, $a^{\text{N}} = 13.4\text{ G}$), and (2) $\bullet\text{OH}$ (DMPO-OH: $a^{\text{H}} = a^{\text{N}} = 14.9\text{ G}$). Fig. 5 shows the EPR spectra of reactants obtained after 1 and 45 min. Neither $\bullet\text{O}_2^-$ nor $\bullet\text{OH}$ was clearly detected in nZVI or S-nZVI suspension after 1 min (Fig. 5a,b). It is likely that at 1 min, nanoparticle addition leads to increase in solution pH (Fig. S5), and the alkaline condition subsequently inhibits Fe(0) dissolution and following Fe(II) leaching (Fig. S8). This result may also imply that FeS on S-nZVI surface could not directly react with O₂ to produce $\bullet\text{O}_2^-$ under alkaline conditions.

After 45 min of reactions, however, characteristic peaks of $\bullet\text{O}_2^-$ and $\bullet\text{OH}$ were detected in both nZVI and S-nZVI suspensions (Fig. 5c,d). The pH, at this point, had decreased to ~ 6.7 (Fig. S5), stimulating O₂ activation by both ionic (Fig. S9) and/or surface bound Fe(II) to produce the radicals (Eqs. (4)–(8)). Moreover, the peak intensities of $\bullet\text{O}_2^-$ and $\bullet\text{OH}$ obtained from nZVI suspension are much lower than those from S-nZVI, which provides a semi-

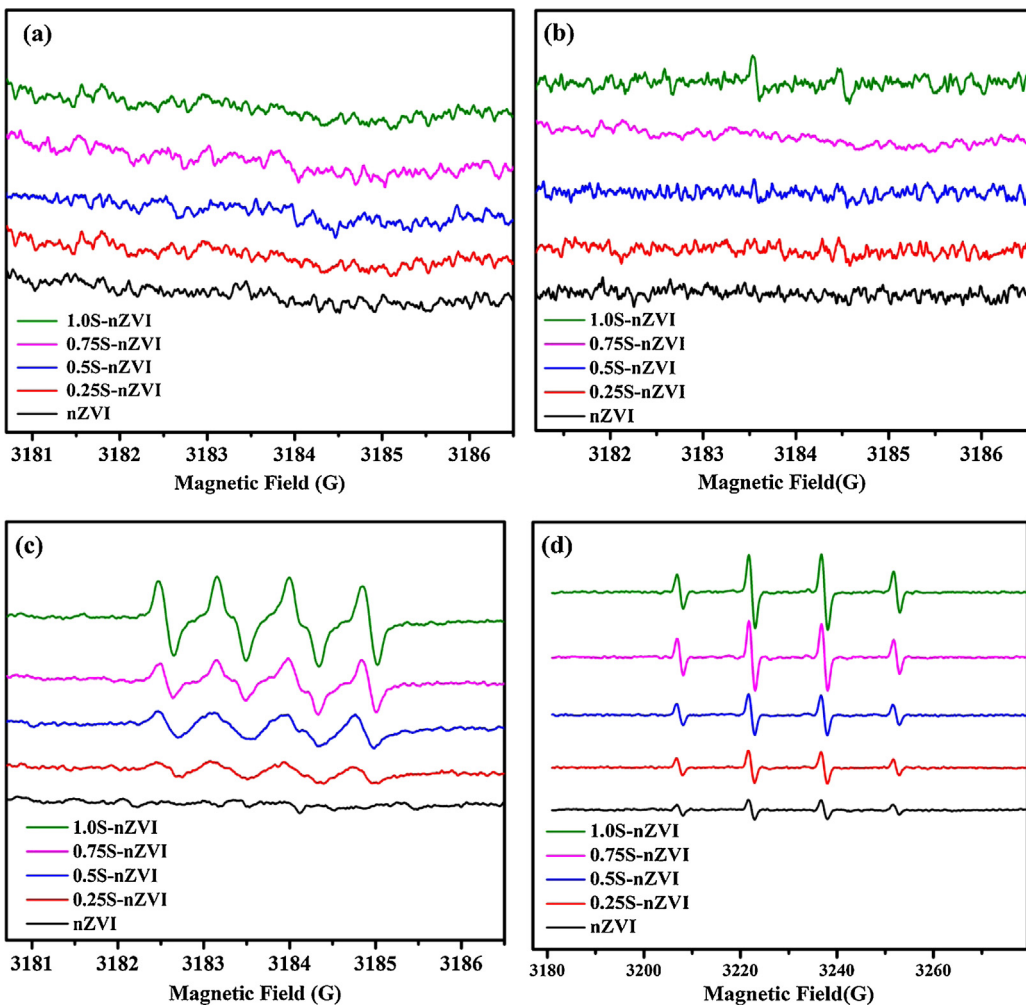
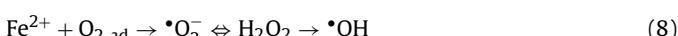
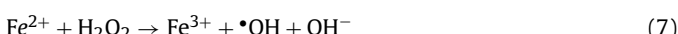
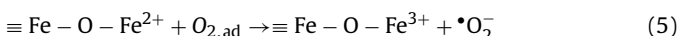
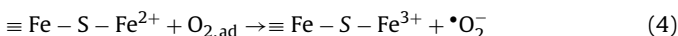


Fig. 5. EPR spectra of different S-nZVI suspensions at different time intervals under aerobic conditions. $\bullet\text{O}_2^-$ (a), and $\cdot\text{OH}$ (b) detected after 1 min; and $\bullet\text{O}_2^-$ (c), and $\cdot\text{OH}$ (d) detected after 45 min. (Reaction condition: DCF = 10 mg/L, S-nZVI = 3.0 g/L).

quantitative indication that the yield of free radicals is higher in the S-nZVI system.



The concentration of ionic Fe(II) in both nZVI and S-nZVI reaction systems are very similar (Fig. S9). As such, the discrepancy in radical yield between both systems is due to differences in the surfaces (shells) of the particles. Based on the literature, higher (additional) yield of radicals by the surface of S-nZVI may be due to the following two reasons:

- 1) Sulfidation greatly restricts the direct reaction between oxygen and nZVI (As shown in Fig. 6), resulting from the more stable Fe-S bond on S-nZVI surface. The Fe-S bonds need to be broken down first, and then form Fe^{2+} and S^{2-} species. These two species can efficiently adsorb O_2 to form peroxide [54]. The low oxidation of $\text{Fe}(0)$ to $\text{Fe}(II)$ by dissolved oxygen in S-nZVI suggests that there will be more $\text{Fe}(0)$ preserved for $\text{Fe}(III)$ reduction later.
- 2) Fe-S cluster functions as an electric "wire" [55], which facilitates electron flow from the $\text{Fe}(0)$ core to the surface/shell $\text{Fe}(III)$. This

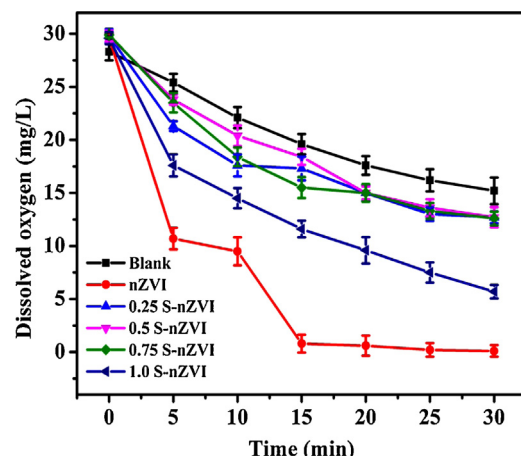
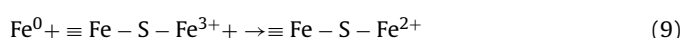


Fig. 6. Effect of sulfidation on oxygen consumption by nZVI.

leads to a continuous formation of surface-bound $\text{Fe}(II)$, which are available for oxygen activation (Eq. (9)).



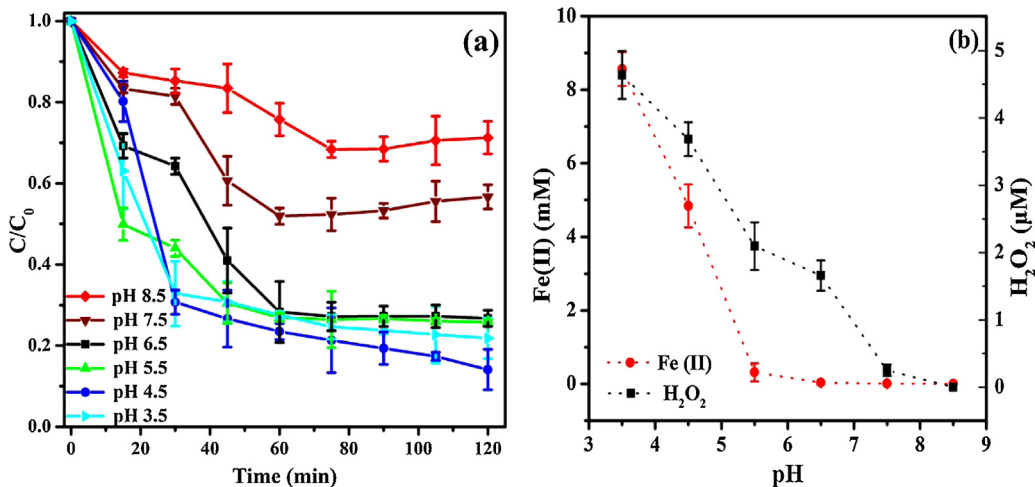


Fig. 7. Removal of DCF at different pH conditions (a), dissolved Fe(II) and H₂O₂ concentrations at different pH conditions (b).

3.5. Effect of pH on DCF removal

It is well-known that Fe(0) dissolution and radical evolution strongly depend on pH. Fig. 7a shows that high removal ratio of DCF can be obtained at pH 3.5–6.5. The removal ratio of DCF significantly increases from 28.8% to 85.9% as solution pH decreases from 8.5 to 4.5, after which it decreases slightly to 78.2% at pH 3.5. Although •O₂⁻ is predominant and can effectively act as a reductive dechlorination radical in alkaline conditions [56], we did not observe DCF removal by S-nZVI at pH 10 (data not shown). This suggests that the dechlorination activity of •O₂⁻ is limited under this condition.

In accordance with the literature, acidic conditions favor Fe dissolution [57] and •OH production (Eq. (7)) [56]. As can be seen in Fig. 7b, the H₂O₂ concentration is negligible at pH 8.5–7.5 due to the deficiency of Fe(II) and H⁺, both of which are needed for its generation [58]. In contrast, although Fe(II) concentration remains extremely low from pH 7.5–5.5, increasing H₂O₂ production was observed. This indicates that aside ionic Fe(II), surface-bound Fe(II) also contributes to H₂O₂ generation. These results imply that S-nZVI can possibly be utilized for aerobic degradation of organic pollutants under neutral pH conditions. Although Fe(II) and H₂O₂ concentrations increase steadily from pH 5.5–3.5, DCF removal ratio initially increases (at pH 5.5–4.5), and then decreases (pH 4.5–3.5). The slight decline in DCF removal below pH 4.5 may be due to rapid S-nZVI dissolution at such low pH conditions. Fig. S10 illustrates that at pH 4.5, 30.6% of S-nZVI dissolved within 15 min (and precipitated after 2 h); while at pH 3.5, 52.7% dissolution was observed (and the dissolved species were relatively stable in solution).

The sharp increase in DCF removal ratio from 43.4% to 73.3% when pH decreases from 7.5 to 6.5 is surprising. We speculate that in addition to enhanced degradation at low pH conditions, DCF adsorption may also play an important role in this phenomenon. As the isoelectric point of γ-FeOOH and Fe₃O₄ is between pH 7.5–6.5 [59], the surface charge of the S-nZVI transformation products changes from negative to positive, which may contribute to DCF adsorption through electrical attractive force.

3.6. Oxidation mechanism

All the studies described in this section were conducted without pH control. Fig. 8 shows the results of quenching experiments. Compared with •O₂⁻ and •SO₄⁻, •OH is a more important ROS in DCF degradation as indicated by a sharp decrease in DCF removal

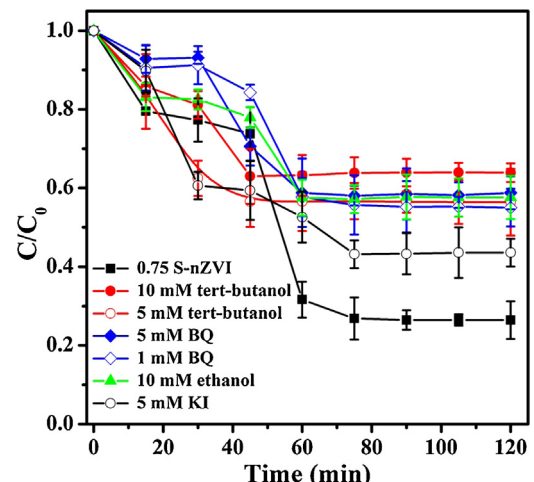


Fig. 8. DCF removal experiments with different quenching reagents.

ratio from 73.5% to 43.6% and 36.1% in the presence of 5 mM and 10 mM tert-butanol (an •OH scavenger), respectively. Furthermore, in the presence of 10 mM ethanol, which scavenges both •SO₄⁻, •OH, decrease in DCF removal (to 42.4%) was similar to when tert-butanol was introduced, meaning that •OH could be main ROS responsible for DCF removal. The EPR spectra results of radicals adducts (Fig. 5) shows no signal of •SO₄⁻, also indicates that •SO₄⁻ is not a very important oxidant in DCF degradation. In the presence of 1 mM and 5 mM BQ (which scavenges •O₂⁻), DCF removal decreases to 45.0% and 41.2%, respectively. Again, these DCF removal values are similar to those observed in the presence of tert-butanol. We propose that •O₂⁻ mainly participates in H₂O₂ generation through one-electron transfer (Eqs. (4)–(8)). This is reported to be the dominant mechanism for •OH generation in the nZVI/O₂ system at neutral pH [15]. These results also imply that H₂O₂ generation through two-electron transfer is negligible in S-nZVI/O₂ system (Eqs. (10) and (11)).

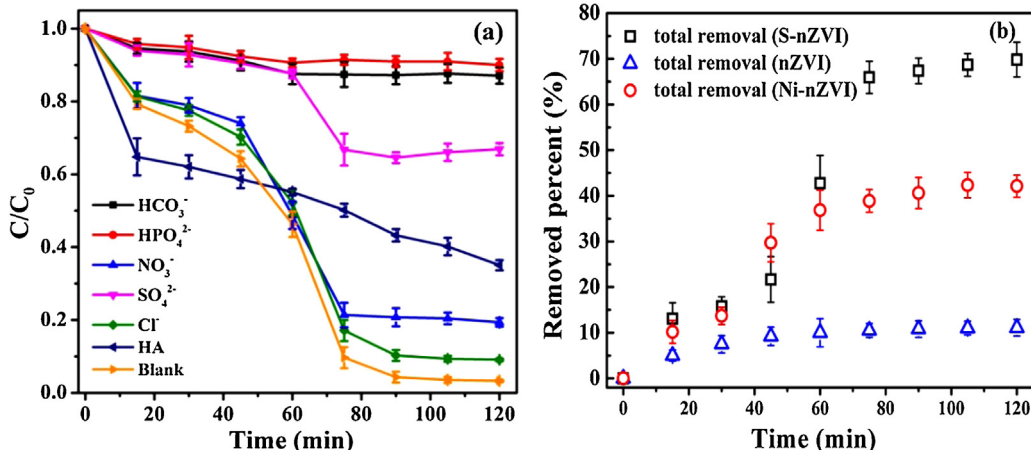


To further examine the role of surface-bound •OH, DCF removal was determined in the presence of iodide ion, which specifically scavenges surface-bounded •OH. The result shows that DCF removal was only 56.4%, less than the removal observed in the presence

Table 2

Summary of DCF removal by iron-based materials under different conditions.

Materials	Reaction conditions	Kinetic rate constants	Removal ratio	Time (min)	Refs.
ZVI	Concentration of DCF = 8.88 mg/L (30 $\mu\text{m}/\text{L}$), Fe = 0.2 g/L, high-frequency ultrasound at 861 kHz, acetate buffered pH = 3.0, and air bubbling in Milli-Q water	1.56 s^{-1}	100%	60	[63,64]
nZVI	Concentration of DCF = 8.88 mg/L (30 $\mu\text{m}/\text{L}$), Fe = 0.2 g/L, high-frequency ultrasound at 861 kHz, acetate buffered pH = 3.0, and air bubbling in Milli-Q water	1.86 s^{-1}	100%	40	[64]
Fe	Concentration of DCF = 10 mg/L (33 $\mu\text{m}/\text{L}$), particles = 40 g/L, pH = 7.5–8.5, oxic condition in distilled water	$3.3 (\pm 4.5) \times 10^{-3} \text{ min}^{-1}$	~32%	120	[65]
PdFe	Concentration of DCF = 10 mg/L (33 $\mu\text{m}/\text{L}$), particles = 40 g/L, pH = 7.5–8.5, oxic condition in distilled water	$12.8 (\pm 5.0) \times 10^{-3} \text{ min}^{-1}$	~82%	120	[65,66]
PdNiFe	Concentration of DCF = 10 mg/L (33 $\mu\text{m}/\text{L}$), particles = 40 g/L, pH = 7.5–8.5, oxic condition in distilled water	$20.2 (\pm 4.5) \times 10^{-3} \text{ min}^{-1}$	100%	120	[66]
nZVI	Concentration of DCF = 10 mg/L (33 $\mu\text{m}/\text{L}$), particles = 3 g/L, initial pH = 6.5, oxic condition in simulated groundwater	N.P. ^a	11%	120	This study
Ni-nZVI	Concentration of DCF = 10 mg/L (33 $\mu\text{m}/\text{L}$), particles = 3 g/L, initial pH = 6.5, oxic condition in simulated groundwater	N.P. ^a	42%	120	This study
S-nZVI	Concentration of DCF = 10 mg/L (33 $\mu\text{m}/\text{L}$), particles = 3 g/L, initial pH = 6.5, oxic condition in simulated groundwater	N.P. ^a	70%	120	This study

^a Not provided (N.P.) due to severe deviation from pseudo-first-order kinetics.**Fig. 9.** DCF removal performance of S-nZVI in solutions with different anions (a), DCF removal performance of three different iron based nanoparticles in simulated groundwater (b).

10 mM *tert*-butanol (Fig. 8). This result indicates that O₂ activation by surface-bound Fe(II) plays an important role in S-nZVI/O₂ system. This is in contrast with Kim et al. [22], which reported that nZVI only served as a source of ionic Fe(II) for hydroxyl radical generation. Similarly, Wang et al. [23], showed that the iron core in Fe@Fe₂O₃ nanowires can provide electrons for the reduction of surface-bound Fe(III), a reliable source of surface-bound Fe(II). Given the higher electrical conductivity of FeS (compared to Fe₂O₃) present in the shell of S-nZVI, it is very likely that the Fe(0) core could serve as electron donor for the reduction of surface-bound Fe(III) to produce surface-bound Fe(II) as shown in Eq. (9). Although different kind of S-nZVI are obtained during the experiments, the XANES analysis shows the Fe(0) content in nZVI and S-nZVI (except the one with molar ratio of S/Fe = 0.4) are all around 80%. The DCF removal ratio observed are different even when equal amounts of the nanoparticles are added into DCF solution (Fig. 4), indicating that Fe(0) is not just a source of ionic Fe(II).

For comparison, we conducted an experiment with commercial FeS obtained from Alfa Aesar (Fig. S11). The DCF removal ability of the commercial FeS was only 19.2%; much lower than nZVI (21.3%) and S-nZVI (73.6%). This shows that FeS alone cannot directly enhance O₂ activation. A previous study found that electron transportation within iron oxide shell would be slower or even blocked as the shell thickness increases [25], which is another evidence that FeS could modify electron flow among iron oxide shell (has been proved in Section 3.4), and subsequently enhanced one-electron transfer.

3.7. DCF removal in stimulated groundwater

Heretofore, the majority of DCF removal studies by iron-based materials were carried out either in distilled water or in acidic conditions (Table 2), which cannot truly represent the capacity of this material. As shown in Table 2, DCF removal capacity of pristine nZVI at neutral pH was limited even though high removal efficiency was

reported in acidic conditions; under pure-water reaction system, metal catalyzed nZVI is able to remove DCF efficiently at near-neutral pH. However, poison of metal catalyst are often reported [60], and some studies even show that the efficiency of iron-H₂O₂ based oxidation would markedly decrease in the presence of common anions [61] and natural organic matters [62].

To test potential application of S-nZVI in pollution remediation, DCF removal in stimulated groundwater was performed. Seen from Fig. 9a, Cl⁻ slightly inhibits DCF removal from 96.7% to 90.9%, while NO₃⁻ and humic acid inhibit it to 80.6% and 64.9%, respectively, when the initial DCF concentration is 3 mg/L. However, the presence of SO₄²⁻, HPO₄²⁻, and HCO₃⁻ decreases DCF removal to 33.1%, 12.9%, and 10.0%, respectively. Inhibition of DCF removal by the anionic species could be attributed to (i) pH increase upon addition of anion, e.g. NO₃⁻, SO₄²⁻, HPO₄²⁻, and HCO₃⁻ (Fig. S12); and (ii) the competitive consumption of ·OH by inorganic anions e.g. SO₄²⁻ and Cl⁻ [67]. Given that there is no clear relationship between aggregation behavior and DCF removal performance, it is very likely that particle aggregation induced by the different anions does not cause decline in DCF removal.

Removal performance of DCF by three different iron based nanoparticles (nZVI, Ni-coated nZVI, and S-nZVI) in a simulated groundwater (pH 6.5) was also investigated (Fig. 9b). The result shows that under aerobic conditions, 69.8% of DCF is removed within 120 min, which is much higher than the efficiency of nZVI (11.0%) and Ni-coated nZVI (42.1%) (reported as an efficient nanomaterial with Ni as catalyst [26]) in a similar condition. This result suggests that the negative influence of common groundwater anions can be alleviated when the pH of the reaction system is below 7.

4. Conclusion

In this study, we produced S-nZVI with various FeS contents. XANES analysis shows that sulfidation stimulates the formation of FeS, but restrains FeOOH generation in particle shell. The increased electrostatic and steric repulsion, and the decreased magnetic attraction resulting from sulfidation alleviate the nanoparticle aggregation, even in the presence of common anions. Under aerobic conditions, S-nZVI is able to remove 73.5% DCF compared to 21.3% removal by nZVI at pH 6.5. Oxidation mechanism studies show that FeS on S-nZVI surface could modify electron transfer in the nanoparticles, resulting in more efficient molecular oxygen activation and ROS production. Fe(0) core in S-nZVI is an important electron donor for surface-bound Fe(III) reduction. This study not only investigated the DCF removal performance of S-nZVI under different conditions, which is crucial for field-scale application of S-nZVI, but also provides new insights on the mechanism of molecular oxygen activation by S-nZVI.

Acknowledgements

This work was funded by international collaborative project (142) from Shanghai Science and Technology Commission (14230710800). The authors would like to thank beamline BL14W1 (Shanghai Synchrotron Radiation Facility) for providing the beam time, the anonymous reviewers for valuable contributions, and Prof. Charles J. Werth for the instructive discussion and help with language.

Appendix A. Supplementary data

Supplementary data associated with this article can be found, in the online version, at <http://dx.doi.org/10.1016/j.apcatb.2016.07.055>.

References

- [1] S. Castiglioni, R. Bagnati, R. Fanelli, F. Pomati, D. Calamari, E. Zuccato, Environ. Sci. Technol. 40 (2006) 357–363.
- [2] Y. Zhang, S.-U. Geissen, C. Gal, Chemosphere 73 (2008) 1151–1161.
- [3] B. Kasprzyk-Hordern, R.M. Dinsdale, A.J. Guwy, Water Res. 42 (2008) 3498–3518.
- [4] M.J. Benotti, R.A. Trenholm, B.J. Vanderford, J.C. Holady, B.D. Stanford, S.A. Snyder, Environ. Sci. Technol. 43 (2008) 597–603.
- [5] N. Vieno, M. Siljanpää, Environ. Int. 69 (2014) 28–39.
- [6] Y. Han, C. Liu, J. Horita, W. Yan, Appl. Catal. B: Environ. 188 (2016) 77–86.
- [7] S. Bae, S. Gim, H. Kim, K. Hanna, Appl. Catal. B: Environ. 182 (2016) 541–549.
- [8] Y. Hwang, P.D. Mines, M.H. Jakobsen, H.R. Andersen, Appl. Catal. B: Environ. 166 (2015) 18–24.
- [9] G. Sheng, P. Yang, Y. Tang, Q. Hu, H. Li, X. Ren, B. Hu, X. Wang, Y. Huang, Appl. Catal. B: Environ. 193 (2016) 189–197.
- [10] G. Sheng, Y. Tang, W. Linghu, L. Wang, J. Li, H. Li, X. Wang, Y. Huang, Appl. Catal. B: Environ. 192 (2016) 268–276.
- [11] Y. Li, W. Cheng, G. Sheng, J. Li, H. Dong, Y. Chen, L. Zhu, Appl. Catal. B: Environ. 174 (2015) 329–335.
- [12] S. Xia, Z. Gu, Z. Zhang, J. Zhang, S.W. Hermanowicz, Chem. Eng. J. 257 (2014) 98–104.
- [13] S.W. Machado, P. Stawinski, A.R. Slonina, J.P. Pinto, H.P. Gross, J.T. Nouws, Albergaria, C. Delerue-Matos, Sci. Total Environ. 461–462 (2013) 323–329.
- [14] C. Noradoun, M.D. Engelmann, M. McLaughlin, R. Hutcheson, K. Breen, A. Paszczynski, I.F. Cheng, Ind. Eng. Chem. Res. 42 (2003) 5024–5030.
- [15] C.R. Keenan, D.L. Sedlak, Environ. Sci. Technol. 42 (2008) 1262–1267.
- [16] S.H. Joo, A.J. Feitz, D.L. Sedlak, T.D. Waite, Environ. Sci. Technol. 39 (2005) 1263–1268.
- [17] S.-Y. Pang, J. Jiang, J. Ma, Environ. Sci. Technol. 45 (2010) 307–312.
- [18] I.A. Katsoyiannis, T. Ruettimann, S.J. Hug, Environ. Sci. Technol. 42 (2008) 7424–7430.
- [19] A.S. Adeleye, L.M. Stevenson, Y. Su, R.M. Nisbet, Y. Zhang, A.A. Keller, Environ. Sci. Technol. 50 (2016) 5597–5605.
- [20] M. Lu, X. Wei, Bioreour. Technol. 102 (2011) 2555–2562.
- [21] C.R. Keenan, D.L. Sedlak, Environ. Sci. Technol. 42 (2008) 6936–6941.
- [22] H.H. Kim, H. Lee, H.E. Kim, J. Seo, S.W. Hong, J.Y. Lee, C. Lee, Water Res. 86 (2015) 66–73.
- [23] L. Wang, M. Cao, Z. Ai, L. Zhang, Environ. Sci. Technol. 48 (2014) 3354–3362.
- [24] C. Lee, C.R. Keenan, D.L. Sedlak, Environ. Sci. Technol. 42 (2008) 4921–4926.
- [25] Z. Ai, Z. Gao, L. Zhang, W. He, J.J. Yin, Environ. Sci. Technol. 47 (2013) 5344–5352.
- [26] C. Lee, D.L. Sedlak, Environ. Sci. Technol. 42 (2008) 8528–8533.
- [27] Y. Nie, S. Xing, C. Hu, J. Qu, Catal. Lett. 142 (2012) 1026–1032.
- [28] R.-A. Doong, Y.-J. Lai, Water Res. 39 (2005) 2309–2318.
- [29] E.J. Kim, J.H. Kim, A.M. Azad, Y.S. Chang, ACS Appl. Mater. Interfaces 3 (2011) 1457–1462.
- [30] Y. Su, A.S. Adeleye, A.A. Keller, Y. Huang, C. Dai, X. Zhou, Y. Zhang, Water Res. 74 (2015) 47–57.
- [31] S.R. Rajajayavel, S. Ghoshal, Water Res. 78 (2015) 144–153.
- [32] C. Carlson, S.M. Hussain, A.M. Schrand, L.K. Braydich-Stolle, K.L. Hess, R.L. Jones, J.J. Schlager, J. Phys. Chem. B 112 (2008) 13608–13619.
- [33] T. Phenrat, N. Saleh, K. Sirk, R.D. Tilton, G.V. Lowry, Environ. Sci. Technol. 41 (2007) 284–290.
- [34] B. Nowack, T.D. Bucheli, Environ. Pollut. 150 (2007) 5–22.
- [35] E.-J. Kim, K. Murugesan, J.-H. Kim, P.G. Tratnyek, Y.-S. Chang, Ind. Eng. Chem. Res. 52 (2013) 9343–9350.
- [36] A.A. Keller, H. Wang, D. Zhou, H.S. Lenihan, G. Cherr, B.J. Cardinale, R. Miller, Z. Ji, Environ. Sci. Technol. 44 (2010) 1962–1967.
- [37] A.S. Adeleye, A.A. Keller, Water Res. 49 (2014) 236–250.
- [38] J. Ma, N.J. Graham, Water Res. 34 (2000) 3822–3828.
- [39] A. Rastogi, S.R. Al-Abed, D.D. Dionysiou, Appl. Catal. B: Environ. 85 (2009) 171–179.
- [40] H. Dong, K. Ahmad, G. Zeng, Z. Li, G. Chen, Q. He, Y. Xie, Y. Wu, F. Zhao, Y. Zeng, Environ. Pollut. 211 (2016) 363–369.
- [41] P.J. Middeldorp, M.A. van Aalst, H.H. Rijnaarts, F.J. Stams, H.F. de Kreuk, G. Schraa, T.N. Bosma, Water Sci. Technol. 37 (1998) 105–110.
- [42] A.E. Harvey Jr., J.A. Smart, E. Amis, Anal. Chem. 27 (1955) 26–29.
- [43] V. Kavitha, K. Palanivelu, Chemosphere 55 (2004) 1235–1243.
- [44] W. Stumm, J.J. Morgan, *Aquatic Chemistry: Chemical Equilibria and Rates in Natural Waters*, John Wiley & Sons, 2012.
- [45] A. Liu, J. Liu, B. Pan, W.-x. Zhang, RSC Adv. 4 (2014) 57377–57382.
- [46] Y. Su, A.S. Adeleye, Y. Huang, X. Zhou, A.A. Keller, Y. Zhang, Sci. Rep. 6 (2016) 26918.
- [47] D. Fan, R.P. Anitori, B.M. Tebo, P.G. Tratnyek, J.S. Lezama Pacheco, R.K. Kukkadapu, M.H. Engelhard, M.E. Bowden, L. Kovarik, B.W. Arey, Environ. Sci. Technol. 47 (2013) 5302–5310.
- [48] Y. Su, A.S. Adeleye, Y. Huang, X. Zhou, A.A. Keller, Y. Zhang, Sci. Rep. 6 (2016) 24358.
- [49] A.S. Adeleye, A.A. Keller, R.J. Miller, H.S. Lenihan, J. Nanopart. Res. 15 (2013) 1–18.
- [50] B. Mukherjee, J.W. Weaver, Environ. Sci. Technol. 44 (2010) 3332–3338.
- [51] Y. Su, A.S. Adeleye, Y. Huang, X. Sun, C. Dai, X. Zhou, Y. Zhang, A.A. Keller, Water Res. 63 (2014) 102–111.

- [52] E. Lefevre, N. Bossa, M.R. Wiesner, C.K. Gunsch, *Sci. Total Environ.* 565 (2016) 889–901.
- [53] A. Liu, J. Liu, W.-x. Zhang, *Chemosphere* 119 (2015) 1068–1074.
- [54] W. Sun, Y.-h. Hu, G.-z. Qiu, W.-q. Qin, *J. Cent. South Univ. Technol.* 11 (2004) 385–390.
- [55] M.-E. Pandelia, W. Nitschke, P. Infossi, M.-T. Giudici-Orticoni, E. Bill, W. Lubitz, *Proc. Natl. Acad. Sci.* 108 (2011) 6097–6102.
- [56] G.-D. Fang, D.D. Dionysiou, S.R. Al-Abed, D.-M. Zhou, *Appl. Catal. B: Environ.* 129 (2013) 325–332.
- [57] Y. Zhang, Y. Su, X. Zhou, C. Dai, A.A. Keller, *J. Hazard. Mater.* 263 (2013) 685–693.
- [58] G.-D. Fang, D.-M. Zhou, D.D. Dionysiou, *J. Hazard. Mater.* 250–251 (2013) 68–75.
- [59] J. Kim, U.G. Nielsen, C.P. Grey, *J. Am. Chem. Soc.* 130 (2008) 1285–1295.
- [60] J. Dunleavy, *Platinum Met. Rev.* 50 (2006) 110.
- [61] G.L. Truong, J. De Laat, B. Legube, *Water Res.* 38 (2004) 2383–2393.
- [62] M.S. Mak, P. Rao, I.M. Lo, *Water Res.* 43 (2009) 4296–4304.
- [63] G.T. Guyer, N.H. Ince, *Ultras. Sonochem.* 18 (2011) 114–119.
- [64] A. Ziyylan, Y. Koltypin, A. Gedanken, N.H. Ince, *Ultras. Sonochem.* 20 (2013) 580–586.
- [65] A. Ghauch, H. Abou Assi, S. Bdeir, *J. Hazard. Mater.* 182 (2010) 64–74.
- [66] A. Ghauch, H.A. Assi, H. Baydoun, A.M. Tuqan, A. Bejjani, *Chem. Eng. J.* 172 (2011) 1033–1044.
- [67] J. De Laat, G. Truong Le, B. Legube, *Chemosphere* 55 (2004) 715–723.